Nonlinear Dyn (2022) 108:1573–1583
https://doi.org/10.1007/s11071-021-07193-6

ORIGINAL PAPER

Valley Hall edge solitons in honeycomb lattice with an armchair-type domain wall

Qian Tang · Milivoj R. Belić · Yi Qi Zhang · Yan Peng Zhang · Yong Dong Li

Received: 6 November 2021 / Accepted: 29 December 2021 / Published online: 12 February 2022

Abstract Thanks to the topological protection, photonic topological edge states can move along the edges of photonic crystals without radiating into the bulk or reflecting when encountering disorders or defects. The valley Hall effect helps obtain topological edge states without breaking the time-reversal symmetry but breaking the inversion symmetry of the system, which means that the valley Hall edge state is independent of the magnetic field. Thus, with two inversion symmetry-broken photonic lattices, a domain wall that supports valley Hall edge states can be established. Generally, the zigzag-type domain wall is likely to support topological valley Hall edge states. However, in this work we investigate the valley Hall edge state on the armchair-type domain wall in a honeycomb lattice and demonstrate that armchair-type valley Hall edge states can also circumvent sharp corners with tiny reflection. The armchair-type domain wall, with the refractive index change being staggered, supports not only the bright but also the dark valley Hall edge solitons, and even the vector valley Hall edge solitons. Our results deepen the understanding of topological valley Hall edge states on different types of domain walls and may find applications in developing techniques of manipulating light fields for fabricating on-chip optical functional devices.

Keywords Valley Hall effect · Honeycomb lattice · Edge state · Soliton

Q. Tang
Ministry of Education Key Laboratory for Nonequilibrium Synthesis and Modulation of Condensed Matter, Shaanxi Province Key Laboratory of Quantum Information and Quantum Optoelectronic Devices, School of Physics, Xi'an Jiaotong University, No. 28 Xianning West Road, Xi'an, 710049, Shaanxi Province, China

M. R. Belić
Science Program, Texas A&M University at Qatar, Doha P.O. Box 23874, Qatar

Y. Q. Zhang (✉)· Y. P. Zhang · Y. D. Li
Key Laboratory for Physical Electronics and Devices of the Ministry of Education & Shaanxi Key Lab of Information Photonic Technique, School of Electronic Science and Engineering, Xi'an Jiaotong University, No. 28 Xianning West Road, Xi'an 710049, Shaanxi Province, China
e-mail: zhangyiqi@xjtu.edu.cn

1 Introduction

Topological insulator is a new phase of matter in which only the surface of the sample is allowed to conduct electrons, with the bulk being completely insulating [1,2]. This peculiar property of the topological insulator is associated with its band structure, where there are edge states distributed in the band gap that connect the bulk bands. To date, the concept of topological insulator has been introduced into other physical branches, such as acoustics [3–8], mechanical systems [9,10], ultracold atoms [11,12], polaritons in microcavities [13–15], electrical circuits [16–21], and photonics [22–31]. In particular, in photonics the "topological insulator" refers to the photonic structure in which light propagates along the edges of the structure, while the bulk

remains in dark. The new field "topological photonics" [32–41] is becoming more and more significant, both in basic science and potential applications, after being more than 10 years in development. The photonic crystal platform offers unique advantages compared to other fields, for example, by introducing nonlinearity [35] and fabricating non-Hermitian configurations, or simply by offering enormous versatility in the choice of various one-, two- and even three-dimensional lattice geometries [36,39,42].

Recent progress in this field indeed demonstrates that the nonlinearity plays an important role and has inspired the emergence of new phenomena in topological photonic systems. Typical examples include topological insulator lasers [43–50], nonlinearity-induced topological transitions and edge solitons [30], and bistability [51,52]. Topological edge solitons are localized bound states moving with constant transverse speed that are only confined to the boundary of the sample, owing to their topological nature. On the one hand, they are immune to defects or disorders when they move along the boundary, because of the topological protection, and on the other hand, they can maintain their envelopes due to nonlinear self-action. However, in the photonic Floquet topological insulators the time-reversal symmetry is broken by the artificial magnetic field, due to the helicity of the waveguide arrays. Hence, the topological closed currents in the bulk originating from the edge states were first reported in theory [53] and then in experiment [29]. The topological edge solitons in Floquet systems were first investigated in depth in discrete [54–56] and then in continuous models [57–60]. In polariton topological insulators, in which the time-reversal symmetry is broken by the authentic magnetic field due to the spin–orbit coupling, the topological edge solitons were also reported first in theory [61–64]. Besides the aforementioned topological edge solitons, Dirac solitons [65], Bragg solitons [66], and valley Hall edge solitons [67–69] have also drawn close scrutiny in various topological systems. Thus far, topologically trivial edge solitons were experimentally realized [70], and the experimental observation of their topological counterparts is still to be explored, even though there were some beneficial attempts [29,67].

Although the valley Hall topological edge solitons have been reported previously, the domain wall adopted in the honeycomb lattice [68] was only of a zigzag type. It is therefore of interest to consider valley Hall edge solitons along other types of domain walls, e.g., in an armchair-type domain wall. This is especially because the edge states appearing along the armchair-type domain are not admitted to be topological [71], since they do not emerge in the bulk band but reside totally in the gap. Thus, the edge states on the armchair-type domain wall are expected to show inter-valley scattering without topological protection. Hence, the purpose of this paper is exactly to investigate and demonstrate valley Hall edge solitons resulting from the valley Hall effect [72] along the armchair-type domain wall.

Nevertheless, we do not want to subvert the accepted opinion that the inter-valley scattering is inexcusable when it comes to circumventing sharp corners. Some radiation still occurs and the topological protection is not provided completely, but it plays a significant part. In addition, this work will show that the edge states on the armchair-type domain walls are not always completely in the bandgap—they may emerge from the bulk bands by adjusting the detuning. Last but not the least, the valley Hall edge solitons on the armchair-type domain wall are investigated here in a detailed way that includes both the bright and dark solitons. We believe this investigation will broaden the understanding of valley Hall edge states on the armchair-type domain wall and enlighten the discussion on potential applications. Therefore, if one chooses an edge state with good localization, the topological property will be sacrificed to the appearance of some inter-valley scattering.

2 Results

2.1 Band structure and linear modes

The propagation of the valley Hall edge state along the longitudinal z axis of the waveguide array with focusing cubic nonlinearity can be described by the dimensionless nonlinear Schrödinger-like paraxial wave equation,

$$i\frac{\partial\psi}{\partial z} = -\frac{1}{2}\left(\frac{\partial^2}{\partial x^2} + \frac{\partial^2}{\partial y^2}\right)\psi - \mathcal{R}(x,y)\psi - |\psi|^2\psi, \tag{1}$$

where ψ is the field amplitude, x and y are the normalized transverse coordinates, and z is the normalized propagation distance. The potential function $\mathcal{R}$ stands for the waveguide array that is arranged within a honeycomb landscape without any modulation along the lon-

gitudinal coordinate. The profiles of individual waveguides in the array are described by Gaussian functions of width σ:

$$\mathcal{R}(x, y) = p_{\mathrm{A,B}} \sum_{m,n} \exp\left[-\frac{(x - x_{m,n})^2 + (y - y_{m,n})^2}{\sigma^2}\right], \quad (2)$$

where $p_{\mathrm{A,B}} \sim \delta n_{\mathrm{A,B}}$ stands for the depths of waveguides in two sublattices, and $(x_{m,n}, y_{m,n})$ are the coordinates of the nodes in the honeycomb grid. We consider a configuration that is periodic along the y axis and is limited along the x axis, with outer boundaries located far away from the domain wall, so that $\mathcal{R}(x, y) = \mathcal{R}(x, y + L)$ with $L = 3d$ and d being the array constant, i.e., the distance between two nearest sites. Representative parameter values for these quantities are $d = 1.4$ and $\sigma = 0.5$. The average refractive index modulation depth is set to be $p_{\mathrm{in}} = 10.3$, while the detuning is $\delta = 0.55$.

The setup is shown in Fig. 1. For the honeycomb array on the left side of the domain wall in Fig. 1c, we set $p_{\mathrm{A}} = p_{\mathrm{in}} + \delta$ and $p_{\mathrm{B}} = p_{\mathrm{in}} - \delta$, while for the array on the right side of the domain wall we assume an inverted detuning, so that $p_{\mathrm{A}} = p_{\mathrm{in}} - \delta$ and $p_{\mathrm{B}} = p_{\mathrm{in}} + \delta$. The domain wall emerging between these two arrays is characterized by the staggered refractive indices, see the red rectangle in Fig. 1c. Assuming that waveguide arrays are prepared by using the femtosecond laser writing technique in fused silica [22,27,29,30,73,74], the normalized parameters described above can be switched to experimental values. Provided the laser radiation at the wavelength of 800 nm is used and the characteristic transverse scale is set to 10 μm that corresponds to dimensionless coordinates $x, y = 1$, the array constant is 14 μm, the waveguide width is 5 μm, and $p_{\mathrm{in}} = 10.3$ corresponds to the refractive index modulation depth of $\sim 1.1 \times 10^{-3}$.

By inserting the ansatz $\psi(x, y, z) = \phi(x, y) \exp(i\beta z)$ with $\phi(x, y) = u(x, y) \exp(ik_y y)$ into Eq. (1) and without considering the nonlinear term, one obtains the eigenvalue problem

$$\beta u = \frac{1}{2}\left(\frac{\partial^2}{\partial x^2} + \frac{\partial^2}{\partial y^2} + 2ik_y \frac{\partial}{\partial y} - k_y^2\right) u + \mathcal{R}u, \quad (3)$$

where $u(x, y) = u(x, y+L)$ is the periodic Bloch wave function, $k_y \in [-\mathrm{K}_y/2, \mathrm{K}_y/2)$ is the Bloch momentum in the first Brillouin zone with $\mathrm{K}_y = 2\pi/L$, and

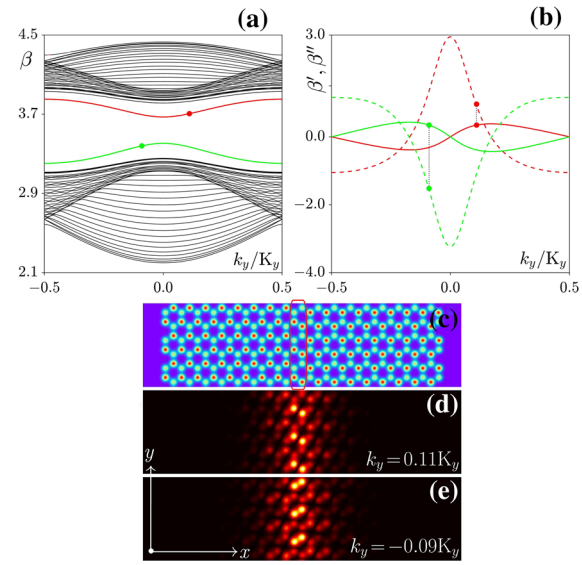

Fig. 1 **a** Band structure of the composite honeycomb lattice with an armchair-type domain wall displayed in (c). Green and red curves are the edge states, and the black curves are the bulk states. **b** First-order β' (solid curves) and second-order β'' (dashed curves) derivatives of the edge states. **c** Composite honeycomb lattice with broken inversion symmetry. The domain wall is of the armchair-type, with staggered refractive index change. **d**, **e** Edge states corresponding to the red and green dots, respectively. The values of k_y are shown in the right-bottom corner of each panel. Parameters are: $p_{\mathrm{in}} = 10.3$, $\delta = 0.55$, $a = 1.4$, and $\sigma = 0.5$

β is the propagation constant of the linear mode that is a function of k_y. Based on the plane-wave expansion method, the band structure corresponding to the composite honeycomb lattice with an armchair-type domain wall is displayed in Fig. 1a, in which there are two edge states in the band gap, as indicated by the red and green curves. The appearance of two edge states is due to the refractive index distribution on the domain wall, which is staggered. The edge states on the red curve mainly localize on the sites with bigger refractive index, and those on the green curve mainly on the sites with smaller refractive index [more details can be found in Fig. 1d and e].

To seek for more intricate properties of these edge states, the first-order derivative $\beta' = d\beta/dk_y$ and the second-order derivative $\beta'' = d^2\beta/dk_y^2$ are explored, as shown in Fig. 1b. As is well known, β' estimates the velocity of the edge state, while β'' is responsible for the dispersion. Around the middle of the first Brillouin zone, one finds that β'' is positive for the edge states on the red curve and negative for those on the

green curve. According to the condition for constructing bright and dark solitons, one may expect to find bright edge solitons based on the edge states on the green curve and dark solitons based on the edge states on the red curve. We choose two states from the red and green curve, respectively, as shown in Fig. 1, and display their profiles in Figs. 1d and e, with the Bloch momenta exhibited in the right-bottom corner of each panel. Since both signs of the first-order derivatives of the two selected edge states are positive, the two edge states as well as their bifurcated solitons will move along the same direction—the negative y axis—during propagation.

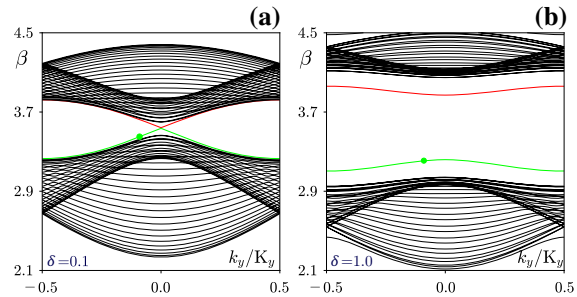

Fig. 2 Band structure of the composite honeycomb lattice with $\delta = 0.1$ **a** and $\delta = 1$ **b**. Other parameters are the same as those adopted in Fig. 1a. Bloch momentum is indicated by the green dots as $k_y = -0.09\mathrm{K}_y$

2.2 Analysis of the inter-valley scattering

As shown in Fig. 1a, the two edge states are completely in the band gap without emerging from the bulk bands. As a result, they are generally classified into defect states rather than the topological edge states, and the inter-valley scattering is predicted when they face defects or disorders during propagation. It is of interest to discuss this "flaw" of the armchair-type valley Hall edge states, answer why the inter-valley scattering happens, and check how strong the inter-valley scattering actually will be.

To this end, we change the detunings and obtain the corresponding band structure, as shown in Fig. 2. One finds that the two edge states are indeed connected with the bulk bands in Fig. 2a, where the detuning is $\delta = 0.1$. But with increasing detuning, the edge states get away from the bulk bands gradually, which is different from those on the zigzag-type domain wall [68] that are always connected with the bulk bands and unaffected by the detunings. Figure 2b shows the band structure with $\delta = 1$ and indeed demonstrates that the edge states are more localized in the band gap than those in Fig. 1a.

Since the edge states seemingly emerge from the bulk bands with small detuning, one question is posed directly—why not use the edge states with small detunings? Before offering an explanation, we first give the answer: the localization of the edge state along the direction that is perpendicular to the domain wall direction is bad.

In Figs. 3a–3c, we show the edge states along the armchair-type domain wall at $k_y = -0.09\mathrm{K}_y$, corresponding to detunings $\delta = 0.1$, $\delta = 0.55$, and $\delta = 1$, respectively. Note that the edge state in Fig. 3b is same as that in Fig. 1e. Indeed, the localization of the edge state in Fig. 3a is the worst. The bigger the detuning, the better the localization of the edge state, and the farther the separation between the edge states and the bulk states. The dilemma for edge states on the armchair-type domain wall is that the system cannot simultaneously guarantee both good localization of the edge states and tight connection between the edge and bulk states.

To display this contradiction more clearly, we also display edge states in the inverted space, as shown by the results in the second row of Fig. 3. The dashed hexagons elucidate the extended first Brillouin zones, in which $\mathbf{K}$ and $\mathbf{K}'$ are the high-symmetric points that are the locations of the "valleys". For the case with $\delta = 0.1$, one finds that the edge state is mainly at the $\mathbf{K}$ point but hardly at the $\mathbf{K}'$ point. However, with increasing detuning, the portion of the energy of the edge state on $\mathbf{K}'$ point also increases. So, for the cases with $\delta = 0.55$ and $\delta = 1$, one observes large amount of energy distributed at the $\mathbf{K}'$ point, which implies that the inter-valley scattering of the edge state can happen easily.

The mixture of the edge state on both $\mathbf{K}$ and $\mathbf{K}'$ points can also be understood in the following way. Since the domain wall is periodic along y axis, only k_y is a good quantum number and the horizontal axis of the band structures in Figs. 1a and 2 is k_y. According to the profile of the first Brillouin zone in Fig. 3, $\mathbf{K}$ and $\mathbf{K}'$ points overlap with each other if one projects the band structure along k_y axis. Ergo, the edge state at a certain Bloch momentum will carry information from both $\mathbf{K}$ and $\mathbf{K}'$ points. For the zigzag-type domain wall, $\mathbf{K}$ and $\mathbf{K}'$ points do not overlap. In this work, we take

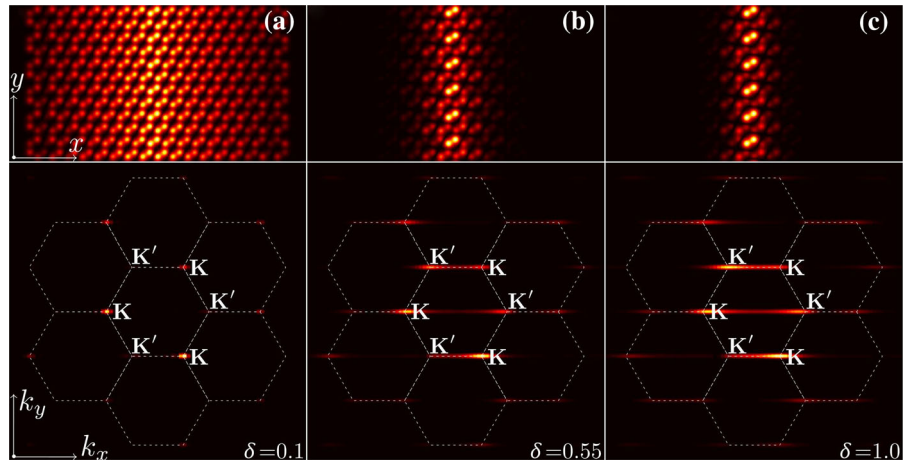

Fig. 3 Amplitude profiles in the real space (first row) and the Fourier space (second row) of linear edge states at $k_y = -0.09\mathrm{K}_y$ but with detunings being $\delta = 0.1$ (**a**), $\delta = 0.55$ (**b**), and $\delta = 1$ (**c**), respectively

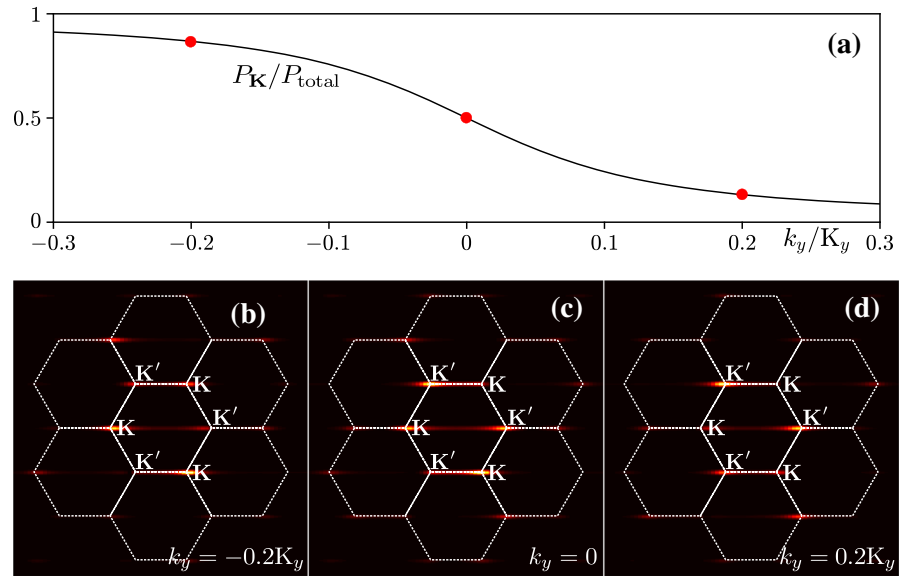

Fig. 4 **a** Ratio of power in the **K** valley versus Bloch momentum k_y. **b–d** Profiles of selected valley Hall edge states at certain Bloch momenta that are shown in the right-bottom corner in each panel, corresponding to the red dots in (a)

the case with $\delta = 0.55$ as a generic example, taking into account the localization of the edge state in both real and inverted spaces.

Investigations also demonstrate that the mixture of the edge states on **K** and **K**′ valleys is also dependent on the Bloch momentum. The power of the edge state in three **K** valleys is denoted as $P_{\mathbf{K}} = \iint_{\mathbf{K}} |\mathcal{F}\{\psi\}|^2 dk_x dk_y$, while the total power in the first Brillouin zone (BZ) is denoted as $P = \iint_{\mathrm{BZ}} |\mathcal{F}\{\psi\}|^2 dk_x dk_y$. Here, $\mathcal{F}$ means the Fourier transform operation. In Fig. 4a, we show the ratio $P_{\mathbf{K}}/P$ as a function of Bloch momentum k_y with fixed $\delta = 0.55$. One finds that the power of the edge state is mainly resident in the **K** valley if $k_y < 0$, and in the **K**′ valley if $k_y > 0$. If $k_y = 0$, the power is equally distributed in **K** and **K**′ valleys. In Fig. 4b–d, we display exemplary edge states in the inverted space at $k_y = -0.2\mathrm{K}_y$, $k_y = 0$, and $k_y = 0.2\mathrm{K}_y$, respectively. Clearly, **K** valley component is dominant in Fig.4b, **K**′ valley is dominant in Fig. 4d, and the two components are equal in Fig. 4c. All in all, if detuning and Bloch momentum are properly chosen, the valley Hall edge state along the armchair-like domain wall can be well topologically protected.

2.3 Valley Hall edge solitons

Even though the edge state on the armchair-type domain wall lies totally in the bandgap, it is interesting to see whether the edge state is reflected by sharp

corners or not. In this section, we first construct solitons based on these "defective" valley Hall edge states and then investigate their propagation dynamics and topological protection.

Following the methods developed in Refs. [60,75], the envelope equations corresponding to Eq. (1) can be written as:

$$i\frac{\partial A}{\partial z} = \frac{\beta''}{2}\frac{\partial^2 A}{\partial Y^2} - \chi|A|^2 A, \tag{4}$$

where A is the slowly-varying envelope, $\chi = \int_{-\infty}^{+\infty} dx \int_0^L |\phi|^4 dy$, and $Y = y + \beta' t$. The soliton solution can be written in the form $\psi(x, y, z) = A(Y, z)\phi(x, y) \exp(i\beta z)$ in which $\phi(x, y)\exp(\beta z)$ is the linear Bloch state. Bright solitons exist in the region $\beta'' < 0$, while dark solitons exist in the region $\beta'' > 0$. Owing to this reason, edge states corresponding to the green and red dots support bright and dark solitons, respectively. Numerically, Eq. (4) can be solved by using Newton method in the form $A(Y, z) = w(Y)\exp(i\beta_{\rm nl} z)$, where $\beta_{\rm nl}$ is the nonlinearity-induced phase shift, which should be sufficiently small to make sure that the profile $w(Y)$ is broad and fulfils the slowly-varying requirement. There are also analytical solutions of Eq. (4):

$$A = \sqrt{2\frac{\beta_{\rm nl}}{\chi}}\,\mathrm{sech}\left(\sqrt{-2\frac{\beta_{\rm nl}}{\beta''}}Y\right)\exp\left(-i\beta_{\rm nl} z\right) \tag{5}$$

for bright solitons and

$$A = \sqrt{\frac{\beta_{\rm nl}}{\chi}}\tanh\left(\sqrt{\frac{\beta_{\rm nl}}{\beta''}}Y\right)\exp\left(-i\beta_{\rm nl} z\right) \tag{6}$$

for dark solitons.

In Fig. 5a, we show the propagation dynamics of the bright valley Hall edge soliton constructed by the linear valley Hall edge state at $k_y = -0.09\mathrm{K}_y$ [see Fig. 1e, and corresponding $\beta'' \approx -1.5503$] superimposed with the envelope at $\beta_{\rm nl} = 0.005$. Launching this soliton into the domain wall of the waveguide array, one finds that it moves along the negative y axis during propagation, without radiating into the bulk. When it propagates to $z = 6000$, its shape is still well maintained. If the nonlinearity in Eq. (1) is lifted, the same incident pulse spreads quickly, and a case in point is the profile at $z = 3000$ shown in Fig. 5b, which almost entirely fills

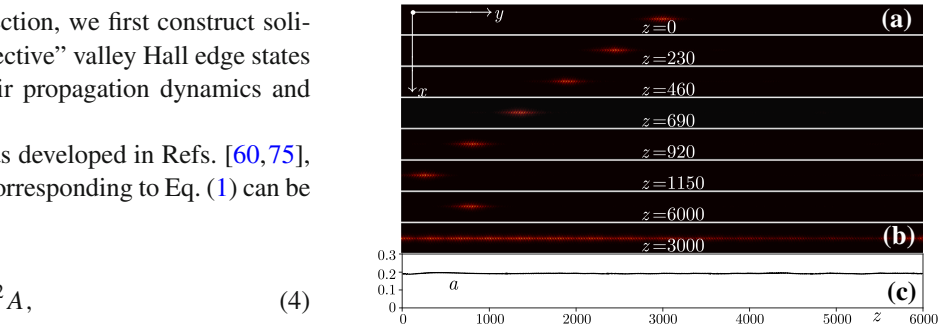

Fig. 5 Propagation dynamics of the bright valley Hall edge soliton. **a** Amplitude profiles of the soliton at selective distances. **b** Amplitude profile of the same input as in (a) at $z = 3000$, after linear propagation. The value of $\beta_{\rm nl}$ is 0.005 and β'' is ~ -1.5503

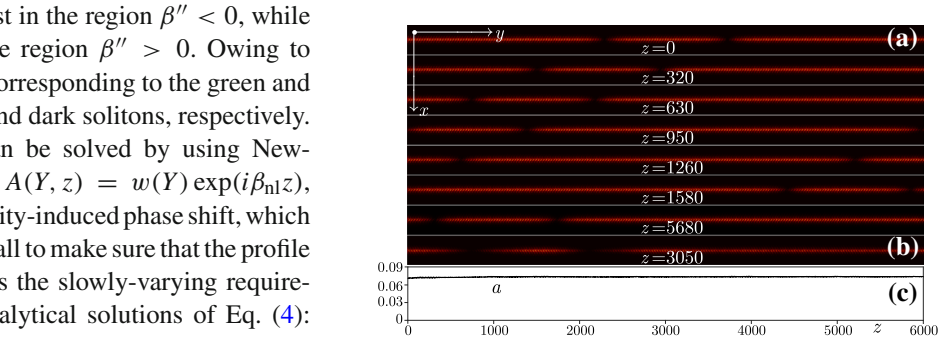

Fig. 6 Same as Fig. 5 but for dark valley Hall edge solitons. The value of $\beta_{\rm nl}$ is 0.0015 and β'' is ~ 0.9231

the domain wall. In addition to the profile, the peak amplitude $a = \max\{|\psi|\}$ in Fig. 5c, which does not reduce upon propagation distance, also demonstrates the self-action (due to nonlinearity) on the valley Hall edge state.

Similar to Fig. 5, we also investigate the dark valley Hall edge soliton based on the valley Hall edge state at $k_y = 0.1\mathrm{K}_y$, and the propagation dynamics is shown in Fig. 6. One finds that the dark valley Hall edge soliton moves along the negative y direction and maintains its profile unchanged during propagation. As a comparison, the linear propagation of the same input is also checked, and the profile at $z = 3050$ is shown in Fig. 6b. One finds that the width of the pulse increases in the absence of nonlinear self-action. For the dark valley Hall edge soliton, we record the peak amplitude of the background $a = \max\{|\psi|\}$ during propagation, as shown in Fig. 6c. It also stays nearly unchanged, even after a long propagation distance.

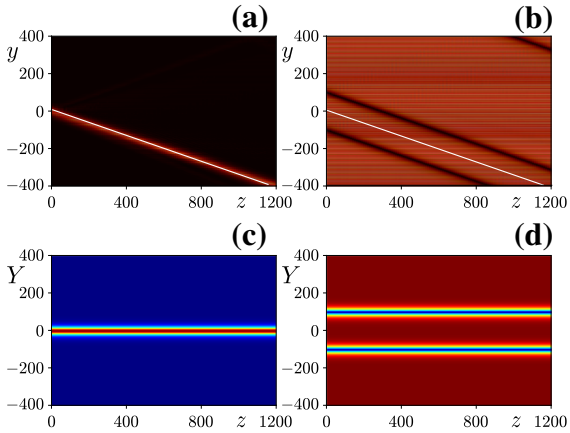

Fig. 7 **a** Amplitude profile of the bright soliton in Fig. 5 at $x = 0$ versus propagation distance z. The slope of the white line shows the moving speed of the soliton along the domain wall, which is $-\beta'$. **b** Setup is as (a), but for the dark soliton in Fig. 6. **c** Propagation of the envelope given in Eq. (5) according to Eq. (4). **d** Setup is as (c), but for the dark envelope in Eq. (6)

Since the solitons in Figs. 5 and 6 are constructed based on the analytical envelopes in Eqs. (5) and (6), it is reasonable to have a direct propagation of the envelopes according to Eq. (4) and have a comparison with the results in Figs. 5 and 6. To better show the whole propagation of bright as well as dark solitons, we record the amplitude of the soliton in the plane $x = 0$, and the corresponding results are shown in Fig. 7a and b. The white line shows the analytical movement of the solitons, with the slope being the moving speed $-\beta'$. Propagations of bright and dark envelopes are exhibited in Fig. 7c and d, in which the coordinate is transformed from y to Y. In consequence, adopting the envelopes to construct edge solitons is valid.

To trace the inter-valley scattering of the edge solitons, an Ω-shaped armchair-type domain wall is established, as shown in Fig. 8a, which displays four sharp corners. A bright soliton is launched into the domain wall, and selective profiles of the edge soliton during propagation are displayed in Fig. 8b. One finds that the bright valley Hall edge soliton can navigate the sharp corners without radiation into the bulk. However, there is some reflection when the soliton circumvents each corner. The transmittance $t = \iint |\psi_{\text{out}}|^2 dxdy / \iint |\psi_{\text{in}}|^2 dxdy > 80\%$ shows that most of the energy can go through sharp corners, which is much higher than that of a topologically trivial state. Not only the bright soliton but also the dark soliton can circumvent sharp corners. In Fig. 9, we exhibit the capability of the dark soliton to navigate an Ω-shaped armchair-type domain wall. Hence, we believe that it is not accurate to dogmatically classify the edge state on armchair-type domain walls as topologically trivial one.

3 Discussion

Until now, we have analyzed the topological properties of the valley Hall edge state on an armchair-type domain wall and obtained both bright and dark solitons. Actually, the first-order derivatives of the edge state corresponding to the green dot and the red dot in Fig. 1b are nearly equal: $\beta' \sim 0.346$, so it makes sense to look for bright-dark vector valley Hall edge solitons along the armchair-type domain walls. In other words, one may obtain both scalar valley Hall edge solitons and vector valley Hall edge solitons, on the armchair-type domain wall. This is an interesting proposition, since one can only obtain scalar solitons if domain wall is zigzag-type [68]. Due to the limitation of the purpose of the work, vector valley Hall edge solitons will be presented in more detail in our future work.

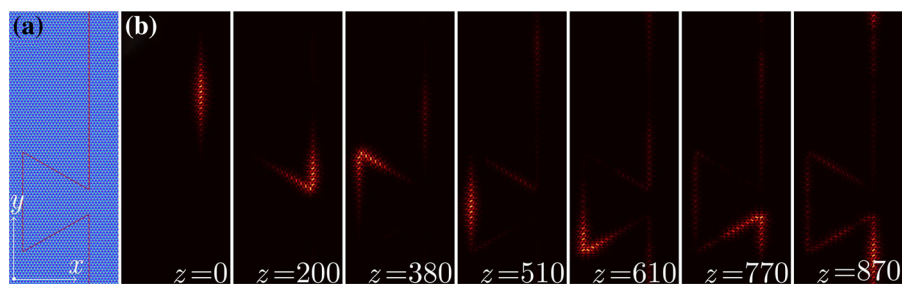

Fig. 8 Topological protection of the bright valley Hall edge soliton. **a** Honeycomb lattice with an Ω-shaped domain wall that is indicated by a red curve. **b** Amplitude profiles of the soliton at selective distances

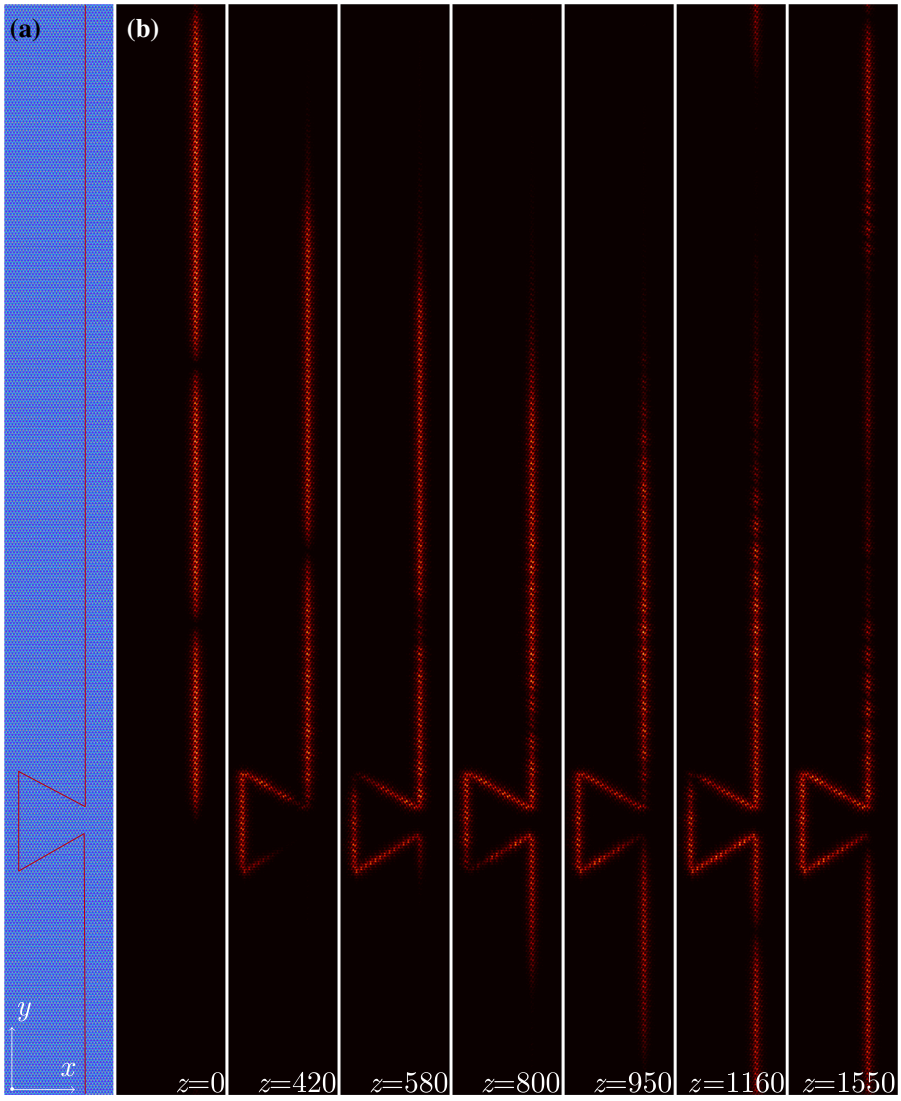

Fig. 9 Setup is as Fig. 8, but for the dark valley Hall edge soliton

4 Conclusion

Summarizing, we have investigated valley Hall edge states along the armchair-type domain wall established in a composite inversion symmetry-broken honeycomb lattice. Valley Hall edge solitons are discussed, and their topological properties are also analyzed. Our results demonstrate that armchair-type valley Hall edge states are neither fully topologically protected, nor completely topologically trivial. They can navigate sharp corners without radiating into the bulk, but with some tiny reflection. Last but not least, the honeycomb lattice with an armchair-type domain wall can serve as an ideal platform for investigating different photonic solitons [76–78].

Acknowledgements This work was supported by the National Natural Science Foundation of China (Nos. 12074308,U1537210) and the Fundamental Research Funds for the Central Universities (Nos. xzy012019038). M. R. B. acknowledges support from the NPRP 11S-1126-170033 project from the Qatar National Research Fund.

Data Availability Statements All data generated or analyzed during this study are included in this published article.

Declarations

Conflicts of interest Not applicable

References

1. Hasan, M.Z., Kane, C.L.: Colloquium: Topological insulators. Rev. Mod. Phys. **82**, 3045–3067 (2010)
2. Qi, X.-L., Zhang, S.-C.: Topological insulators and superconductors. Rev. Mod. Phys. **83**, 1057–1110 (2011)
3. Yang, Z., Gao, F., Shi, X., Lin, X., Gao, Z., Chong, Y., Zhang, B.: Topological acoustics. Phys. Rev. Lett. **114**, 114301 (2015)
4. Peng, Y.-G., Qin, C.-Z., Zhao, D.-G., Shen, Y.-X., Xu, X.-Y., Bao, M., Jia, H., Zhu, X.-F.: Experimental demonstration of anomalous Floquet topological insulator for sound. Nat. Commun. **7**(1), 13368 (2016)
5. He, C., Ni, X., Ge, H., Sun, X.-C., Chen, Y.-B., Lu, M.-H., Liu, X.-P., Chen, Y.-F.: Acoustic topological insulator and robust one-way sound transport. Nat. Phys. **12**, 1124–1129 (2016)
6. Lu, J., Qiu, C., Ye, L., Fan, X., Ke, M., Zhang, F., Liu, Z.: Observation of topological valley transport of sound in sonic crystals. Nat. Phys. **13**(4), 369–374 (2017)
7. Zhang, X., Xiao, M., Cheng, Y., Lu, M.-H., Christensen, J.: Topological sound. Commun. Phys. **1**(1), 97 (2018)
8. Ma, G., Xiao, M., Chan, C.T.: Topological phases in acoustic and mechanical systems. Nat. Rev. Phys. **1**(4), 281–294 (2019)
9. Süsstrunk, R., Huber, S.D.: Observation of phononic helical edge states in a mechanical topological insulator. Science **349**(6243), 47–50 (2015)
10. Huber, S.D.: Topological mechanics. Nat. Phys. **12**(7), 621–623 (2016)
11. Goldman, N., Dalibard, J., Dauphin, A., Gerbier, F., Lewenstein, M., Zoller, P., Spielman, I.B.: Direct imaging of topological edge states in cold-atom systems. Proc. Natl. Acad. Sci. **110**(17), 6736–6741 (2013)
12. Jotzu, G., Messer, M., Desbuquois, R., Lebrat, M., Uehlinger, T., Greif, D., Esslinger, T.: Experimental realisation of the topological Haldane model. Nature **515**, 237–240 (2014)
13. Nalitov, A.V., Solnyshkov, D.D., Malpuech, G.: Polariton $\mathbb{Z}$ topological insulator. Phys. Rev. Lett. **114**, 116401 (2015)
14. St-Jean, P., Goblot, V., Galopin, E., Lemaître, A., Ozawa, T., Le Gratiet, L., Sagnes, I., Bloch, J., Amo, A.: Lasing in topological edge states of a one-dimensional lattice. Nat. Photon. **11**(10), 651–656 (2017)
15. Klembt, S., Harder, T.H., Egorov, O.A., Winkler, K., Ge, R., Bandres, M.A., Emmerling, M., Worschech, L., Liew, T.C.H., Segev, M., Schneider, C., Höfling, S.: Exciton-polariton topological insulator. Nature **562**(7728), 552–556 (2018)
16. Albert, V.V., Glazman, L.I., Jiang, L.: Topological properties of linear circuit lattices. Phys. Rev. Lett. **114**, 173902 (2015)
17. Hadad, Y., Soric, J.C., Khanikaev, A.B., Alù, A.: Self-induced topological protection in nonlinear circuit arrays. Nat. Electron. **1**(3), 178–182 (2018)
18. Imhof, S., Berger, C., Bayer, F., Brehm, J., Molenkamp, L.W., Kiessling, T., Schindler, F., Lee, C.H., Greiter, M., Neupert, T., Thomale, R.: Topolectrical-circuit realization of topological corner modes. Nat. Phys. **14**(9), 925–929 (2018)
19. Olekhno, N.A., Kretov, E.I., Stepanenko, A.A., Ivanova, P.A., Yaroshenko, V.V., Puhtina, E.M., Filonov, D.S., Cappello, B., Matekovits, L., Gorlach, M.A.: Topological edge states of interacting photon pairs emulated in a topolectrical circuit. Nat. Commun. **11**(1), 1436 (2020)
20. Helbig, T., Hofmann, T., Imhof, S., Abdelghany, M., Kiessling, T., Molenkamp, L.W., Lee, C.H., Szameit, A., Greiter, M., Thomale, R.: Generalized bulk-boundary correspondence in non-Hermitian topolectrical circuits. Nat. Phys. **16**(7), 747–750 (2020)
21. Li, R., Lv, B., Tao, H., Shi, J., Chong, Y., Zhang, B., Chen, H.: Ideal type-II Weyl points in topological circuits. National Sci. Rev. **8**(7), 192 (2020)
22. Rechtsman, M.C., Zeuner, J.M., Plotnik, Y., Lumer, Y., Podolsky, D., Dreisow, F., Nolte, S., Segev, M., Szameit, A.: Photonic Floquet topological insulators. Nature **496**, 196–200 (2013)
23. Haldane, F.D.M., Raghu, S.: Possible realization of directional optical waveguides in photonic crystals with broken time-reversal symmetry. Phys. Rev. Lett. **100**, 013904 (2008)
24. Wang, Z., Chong, Y., Joannopoulos, J.D., Soljačić, M.: Observation of unidirectional backscattering-immune topological electromagnetic states. Nature **461**, 772–775 (2009)
25. Lindner, N.H., Refael, G., Galitski, V.: Floquet topological insulator in semiconductor quantum wells. Nat. Phys. **7**(6), 490–495 (2011)
26. Hafezi, M., Demler, E.A., Lukin, M.D., Taylor, J.M.: Robust optical delay lines with topological protection. Nat. Phys. **7**(11), 907–912 (2011)
27. Stützer, S., Plotnik, Y., Lumer, Y., Titum, P., Lindner, N.H., Segev, M., Rechtsman, M.C., Szameit, A.: Photonic topological Anderson insulators. Nature **560**(7719), 461–465 (2018)
28. Yang, Y., Gao, Z., Xue, H., Zhang, L., He, M., Yang, Z., Singh, R., Chong, Y., Zhang, B., Chen, H.: Realization of a three-dimensional photonic topological insulator. Nature **565**(7741), 622–626 (2019)
29. Mukherjee, S., Rechtsman, M.C.: Observation of Floquet solitons in a topological bandgap. Science **368**(6493), 856–859 (2020)
30. Maczewsky, L.J., Heinrich, M., Kremer, M., Ivanov, S.K., Ehrhardt, M., Martinez, F., Kartashov, Y.V., Konotop, V.V., Torner, L., Bauer, D., Szameit, A.: Nonlinearity-induced photonic topological insulator. Science **370**(6517), 701–704 (2020)
31. Yang, Z., Lustig, E., Lumer, Y., Segev, M.: Photonic Floquet topological insulators in a fractal lattice. Light Sci. Appl. **9**(1), 128 (2020)
32. Lu, L., Joannopoulos, J.D., Soljačić, M.: Topological photonics. Nat. Photon. **8**(11), 821–829 (2014)
33. Ozawa, T., Price, H.M., Amo, A., Goldman, N., Hafezi, M., Lu, L., Rechtsman, M.C., Schuster, D., Simon, J., Zilberberg, O., Carusotto, I.: Topological photonics. Rev. Mod. Phys. **91**, 015006 (2019)
34. Kim, M., Jacob, Z., Rho, J.: Recent advances in 2D, 3D and higher-order topological photonics. Light Sci. Appl. **9**(1), 130 (2020)
35. Smirnova, D., Leykam, D., Chong, Y., Kivshar, Y.: Nonlinear topological photonics. Appl. Phys. Rev. **7**(2), 021306 (2020)
36. Ota, Y., Takata, K., Ozawa, T., Amo, A., Jia, Z., Kante, B., Notomi, M., Arakawa, Y., Iwamoto, S.: Active topological photonics. Nanophoton. **9**(3), 547–567 (2020)

37. Leykam, D., Yuan, L.: Topological phases in ring resonators: recent progress and future prospects. Nanophoton. **9**(15), 4473–4487 (2020)
38. Segev, M., Bandres, M.A.: Topological photonics: where do we go from here? Nanophoton. **10**(1), 425–434 (2021)
39. Parto, M., Liu, Y.G.N., Bahari, B., Khajavikhan, M., Christodoulides, D.N.: Non-Hermitian and topological photonics: optics at an exceptional point. Nanophoton. **10**(1), 403–423 (2021)
40. Wang, H., Gupta, S.K., Xie, B., Lu, M.: Topological photonic crystals: a review. Front. Optoelectron. **13**(1), 50–72 (2020)
41. Liu, H., Xie, B., Cheng, H., Tian, J., Chen, S.: Topological photonic states in artificial microstructures [Invited]. Chin. Opt. Lett. **19**(11), 052602 (2021)
42. Xia, S., Kaltsas, D., Song, D., Komis, I., Xu, J., Szameit, A., Buljan, H., Makris, K.G., Chen, Z.: Nonlinear tuning of PT symmetry and non-Hermitian topological states. Science **372**(6537), 72–76 (2021)
43. Harari, G., Bandres, M.A., Lumer, Y., Rechtsman, M.C., Chong, Y.D., Khajavikhan, M., Christodoulides, D.N., Segev, M.: Topological insulator laser: theory. Science **359**(6381), 4003 (2018)
44. Bandres, M.A., Wittek, S., Harari, G., Parto, M., Ren, J., Segev, M., Christodoulides, D.N., Khajavikhan, M.: Topological insulator laser: experiments. Science **359**(6381), 4005 (2018)
45. Dikopoltsev, A., Harder, T.H., Lustig, E., Egorov, O.A., Beierlein, J., Wolf, A., Lumer, Y., Emmerling, M., Schneider, C., Höfling, S., Segev, M., Klembt, S.: Topological insulator vertical-cavity laser array. Science **373**(6562), 1514–1517 (2021)
46. Bahari, B., Ndao, A., Vallini, F., El Amili, A., Fainman, Y., Kanté, B.: Nonreciprocal lasing in topological cavities of arbitrary geometries. Science **358**(6363), 636–640 (2017)
47. Kartashov, Y.V., Skryabin, D.V.: Two-dimensional topological polariton laser. Phys. Rev. Lett. **122**, 083902 (2019)
48. Zeng, Y., Chattopadhyay, U., Zhu, B., Qiang, B., Li, J., Jin, Y., Li, L., Davies, A.G., Linfield, E.H., Zhang, B., Chong, Y., Wang, Q.J.: Electrically pumped topological laser with valley edge modes. Nature **578**(7794), 246–250 (2020)
49. Zhong, H., Li, Y.D., Song, D.H., Kartashov, Y.V., Zhang, Y.Q., Zhang, Y.P., Chen, Z.: Topological valley Hall edge state lasing. Laser Photon. Rev. **14**(7), 2000001 (2020)
50. Gong, Y., Wong, S., Bennett, A.J., Huffaker, D.L., Oh, S.S.: Topological insulator laser using valley-hall photonic crystals. ACS Photon. **7**(8), 2089–2097 (2020)
51. Kartashov, Y.V., Skryabin, D.V.: Bistable topological insulator with exciton-polaritons. Phys. Rev. Lett. **119**, 253904 (2017)
52. Zhang, W., Chen, X., Kartashov, Y.V., Skryabin, D.V., Ye, F.: Finite-dimensional bistable topological insulators: From small to large. Laser Photon. Rev. **13**(11), 1900198 (2019)
53. Lumer, Y., Plotnik, Y., Rechtsman, M.C., Segev, M.: Self-localized states in photonic topological insulators. Phys. Rev. Lett. **111**, 243905 (2013)
54. Ablowitz, M.J., Curtis, C.W., Ma, Y.-P.: Linear and nonlinear traveling edge waves in optical honeycomb lattices. Phys. Rev. A **90**, 023813 (2014)
55. Ablowitz, M.J., Cole, J.T.: Tight-binding methods for general longitudinally driven photonic lattices: edge states and solitons. Phys. Rev. A **96**, 043868 (2017)
56. Ablowitz, M.J., Ma, Y.-P.: Strong transmission and reflection of edge modes in bounded photonic graphene. Opt. Lett. **40**(20), 4635–4638 (2015)
57. Leykam, D., Chong, Y.D.: Edge solitons in nonlinear-photonic topological insulators. Phys. Rev. Lett. **117**, 143901 (2016)
58. Ivanov, S.K., Kartashov, Y.V., Maczewsky, L.J., Szameit, A., Konotop, V.V.: Edge solitons in Lieb topological Floquet insulator. Opt. Lett. **45**(6), 1459–1462 (2020)
59. Ivanov, S.K., Kartashov, Y.V., Maczewsky, L.J., Szameit, A., Konotop, V.V.: Bragg solitons in topological Floquet insulators. Opt. Lett. **45**(8), 2271–2274 (2020)
60. Ivanov, S.K., Kartashov, Y.V., Szameit, A., Torner, L., Konotop, V.V.: Vector topological edge solitons in Floquet insulators. ACS Photon. **7**(3), 735–745 (2020)
61. Kartashov, Y.V., Skryabin, D.V.: Modulational instability and solitary waves in polariton topological insulators. Optica **3**(11), 1228–1236 (2016)
62. Gulevich, D.R., Yudin, D., Skryabin, D.V., Iorsh, I.V., Shelykh, I.A.: Exploring nonlinear topological states of matter with exciton-polaritons: edge solitons in kagome lattice. Sci. Rep. **7**(1), 1780 (2017)
63. Li, C., Ye, F., Chen, X., Kartashov, Y.V., Ferrando, A., Torner, L., Skryabin, D.V.: Lieb polariton topological insulators. Phys. Rev. B **97**, 081103 (2018)
64. Zhang, Y.Q., Kartashov, Y.V., Ferrando, A.: Interface states in polariton topological insulators. Phys. Rev. A **99**, 053836 (2019)
65. Smirnova, D.A., Smirnov, L.A., Leykam, D., Kivshar, Y.S.: Topological edge states and gap solitons in the nonlinear Dirac model. Laser Photon. Rev. **13**(12), 1900223 (2019)
66. Zhang, W., Chen, X., Kartashov, Y.V., Konotop, V.V., Ye, F.: Coupling of edge states and topological Bragg solitons. Phys. Rev. Lett. **123**, 254103 (2019)
67. Zhong, H., Xia, S., Zhang, Y., Li, Y., Song, D., Liu, C., Chen, Z.: Nonlinear topological valley Hall edge states arising from type-II Dirac cones. Adv. Photon. **3**(5), 056001 (2021)
68. Ren, B., Wang, H., Kompanets, V.O., Kartashov, Y.V., Li, Y., Zhang, Y.: Dark topological valley Hall edge solitons. Nanophoton. **10**(13), 3559–3566 (2021)
69. Smirnova, D.A., Smirnov, L.A., Smolina, E.O., Angelakis, D.G., Leykam, D.: Gradient catastrophe of nonlinear photonic valley-Hall edge pulses. Phys. Rev. Research **3**, 043027 (2021)
70. Zhang, Z.Y., Wang, R., Zhang, Y.Q., Kartashov, Y.V., Li, F., Zhong, H., Guan, H., Gao, K., Li, F.L., Zhang, Y.P., Xiao, M.: Observation of edge solitons in photonic graphene. Nat. Commun. **11**(1), 1902 (2020)
71. Ma, J., Xi, X., Sun, X.: Topological photonic integrated circuits based on valley kink states. Laser Photon. Rev. **13**(12), 1900087 (2019)
72. Liu, J.-W., Shi, F.-L., He, X.-T., Tang, G.-J., Chen, W.-J., Chen, X.-D., Dong, J.-W.: Valley photonic crystals. Adv. Phys. X **6**(1), 1905546 (2021)
73. Kirsch, M.S., Zhang, Y., Kremer, M., Maczewsky, L.J., Ivanov, S.K., Kartashov, Y.V., Torner, L., Bauer, D., Szameit,

A., Heinrich, M.: Nonlinear second-order photonic topological insulators. Nat. Phys. **17**(9), 995–1000 (2021)
74. Tan, D., Wang, Z., Xu, B., Qiu, J.: Photonic circuits written by femtosecond laser in glass: improved fabrication and recent progress in photonic devices. Adv. Photon. **3**(11), 024002 (2021)
75. Ivanov, S.K., Kartashov, Y.V., Heinrich, M., Szameit, A., Torner, L., Konotop, V.V.: Topological dipole Floquet solitons. Phys. Rev. A **103**, 053507 (2021)
76. Kartashov, Y.V., Astrakharchik, G.E., Malomed, B.A., Torner, L.: Frontiers in multidimensional self-trapping of nonlinear fields and matter. Nat. Rev. Phys. **1**(3), 185–197 (2019)
77. Malomed, B.A., Mihalache, D.: Nonlinear waves in optical and matter-wave media: a topical survey of recent theoretical and experimental results. Rom. J. Phys. **64**(5–6), 106 (2019)
78. Mihalache, D.: Localized structures in optical and matter-wave media: a selection of recent studies. Rom. Rep. Phys. **73**(2), 403 (2021)